Mathematical Modeling of the Role of *Survivin* on Dedifferentiation and Radioresistance in Cancer

Adam Rhodes, Thomas Hillen

April 30, 2016

Centre for Mathematical Biology, University of Alberta, Canada
arhodes@ualberta.ca, thillen@ualberta.ca

Abstract: We use a mathematical model to investigate cancer resistance to radiation, based on dedifferentiation of non stem cancer cells into cancer stem cells. Experimental studies by Iwasa 2008, using human non small cell lung cancer (NSCLC) cell lines in mice, have implicated the inhibitor of apoptosis protein (IAP) *survivin* in cancer resistance to radiation. A marked increase in radio-sensitivity was observed after inhibiting survivin expression with a specific survivin inhibitor YM155 (*sepantronium bromide*). It was suggested that these observations are due to survivin-dependent dedifferentiation of non-stem cancer cells into cancer stem cells. Here, we confirm this hypothesis with a mathematical model, which we fit to Iwasa's data on NSCLC in mice. We investigate the timing of combination therapies of YM155 administration and radiation. We find an interesting dichotomy. Sometimes it is best to hit a cancer with a large radiation dose right at the beginning of the YM155 treatment, while in other cases, it appears advantageous to wait a few days until most cancer cells are sensitized, and then radiate. The optimal strategy depends on the nature of the cancer and the dose of radiation administered.

1 Introduction

For many cancers, radiation therapy has become a standard component of treatment. Its effectiveness, however, is often only palliative as a result of radioresistance. While the mechanism responsible for radioresistance remains unknown, the cancer stem

cell hypothesis may provide some insight. In the cancer stem cell model of cancer, tumors are heterogeneous cell populations, organized in a hierarchcical fashion [24]. Self-renewing and tumorigenic cancer stem cells (CSCs), also known as tumor-initiating cells, are located at the apex of the cell lineage, and are capable of both, self-renewal and production of more differentiated, less tumorigenic non-stem cancer cells (NSCCs). The latter property of CSCs is, in fact, their defining property - the ability to, when isolated, reproduce a heterogeneous tumor. From their initial discovery in acute myeloid luekemia [33], CSCs have since been identified in a number of cancers, including lung cancer [18]- both small cell (SCLC) [45] and non-small cell (NSCLC) [50] - breast [3], brain [47], and pancreas [36] among others. Adding to their importance when it comes to tumor progression is the observation that CSCs are relatively resistant to radiotherapy when compared to their non-stem counterparts [2, 9, 41], possibly accounting for rapid recurrence upon termination of treatment.

In this paper, we set out to investigate the potential role of cancer stem cell dedifferentiation, the role of *survivin* in NSCC dedifferentiation and the control of *survivin* by the *survivin* inhibitor YM155 (sepantronium bromide). Our mathematical model is based on recent experimental data of Iwasa et al. [27] on non small cell lung cancer (NSCLC) in mice. They consider four treatment regimens: (i) a control treatment in which the tumor was allowed to grow without interference, (ii) a γ-radiation treatment of $10Gy$ in $2Gy$ fractions for 5 days, (iii) a YM155 treatment in which the *survivin* inhibitor YM155 was administered by continuous IV infusion over the course of 7 days, and (iv) a combination therapy, which combines the above radiation and YM155 treatments. Tumor volumes were measured over the course of treatment. Iwasa et al. [27] could show that both treatments, (ii) and (iii), had some effect on tumor growth. However, a combination, (iv), had a much larger effect on tumor control. Here we argue based on our model, that the increased effect of treatment (iv) can be related to the dedifferentiation effect of *survivin*, as previously suggested by Dahan et al. [13]. Survivin appears to be released after radiation damage and it promotes NSCC to become CSC. Consequently, they are less sensitive to radiation damage. The addition of YM155 inhibits *survivin* production and reduces the number of CSC, making the tumor more sensitive to radiation.

We develop a system of ordinary differential equations (ODEs) to help elucidate the dynamics between CSCs, NSCCs, and *survivin*. We use two variants of the model - one that assumes a constant rate of dedifferentiation (CD-model) and the other incorporating a *survivin*-dependent rate of dedifferentiation (SDD-model) - to investigate the role of *survivin* in radioresistance in CSC driven tumors. We use the (corrected) Akaike Information Criterion (AICc) to fit the two models to the data from Iwasa et al. [27] and compare the resulting fits. We find that the model incorporating a *survivin*-dependent rate of dedifferentiation (SDD) offers a better explanation of the data. In doing so, we confirm Iwasa's results that a combination of radiation treatment with *survivin* inhibition can significantly increase treatment success. We then use the fit model to investigate various radiation schedules on tumor control and conclude that radiation fractionation scheduling can play a significant role in tumor control. To the

authors' knowledge, this is the first attempt to model the effectiveness of a combination of dedifferentiation and radiation therapy, and provides evidence that such a strategy may be an interesting avenue for further research.

1.1 Dedifferentiation

Traditionally, the conversion dynamics between stem cells and non-stem cells has been assumed rigidly unidirectional, wherein a stem cell can differentiate into a non-stem cell, but the reverse transition cannot occur - once a non-stem cell, always a non-stem cell. This rigid hierarchy in normal (healthy) stem cell dynamics was brought into question with the groundbreaking work of Takahashi et al. [49] where the authors demonstrated that the reverse process - a non-stem cell becoming a stem cell - was possible upon the introduction of four transcription factors (Oct3/4, Sox2, Klf4, and c-Myc). This plastic reversion, or *dedifferentiation*, was subsequently observed *in-vivo* [12], and it is now hypothesized that all non-stem cells are, in principle, capable of dedifferentiating, but very few manage to complete the process [52].

This bidirectional plasticity observed in normal stem cell biology has been translated and incorporated into the CSC hypothesis, with initial experimental manipulations (reviewed in [38]) and subsequent experimental observations [12,30,32] confirming bidirectional plasticity as a key factor in the dynamics of CSC driven tumor growth. Particularly pertinent to radioresistance are the observations that dedifferentiation appears to be induced by clinically relevant doses of radiation [13]. Such radiation-induced dedifferentiation may account for radioresistance by increasing a tumor's radioresistant CSC population.

The mechanisms responsible for the phenotypic plasticity remain poorly understood, but recent evidence [13] implicated the inhibitor of apoptosis protein (IAP) *survivin* (also known as baculoviral inhibitor of apoptosis repeat-containing 5 (BIRC5)) to play a role in the dedifferentiation process. *Survivin* expression is minimal in healthy cells, where the protein plays a role in inhibition of apoptosis (programmed cell death) and mitotic progression [5]. In contrast, the protein is highly expressed in embryonic and fetal tissues as well as in the cells of a variety of cancers including cancers of the lung, breast, brain, and pancreas (see the review in [5]). Even amongst cancer cells, *survivin* is overexpressed by CSCs compared to NSCCs and its' expression levels increase in response to clinically relevant doses of radiation. This has been associated with radiation induced dedifferentiation [13].

The increased expression of *survivin* in response to radiation may be related to the mitochondrial pool of *survivin* [16]. Not only does this pool grow in size in response to radiation, but the *survivin*, together with other cell death regulators housed in the mitochondria, is likely released into the tumor environment upon initiation of radiation-induced apoptosis [16]. Once released, it is then able to interact with the surrounding cancer cells, and may play a role in dedifferentiation. Indeed, by inhibiting radiation-induced *survivin* expression, Dahan et al. [13] showed a marked decrease in differentiation markers (GFAP) together with a marked increase in a variety of stem

markers (Olig2, Sox2, Nestin, A2B5, Nanog, and Notch1), suggesting that the IAP *survivin* plays a critical role in the dedifferentiation process.

The discrepancy in *survivin* expression levels between healthy and cancerous cells has made the protein a promising target for anti-cancer therapies (see the review in [40]). One strategy investigated has been to prevent the transcription of the *survivin* gene, thereby suppressing the expression of *survivin* at the protein level. Nakahara and colleagues [39] discovered the small molecule *survivin* inhibitor YM155 accomplished precisely this and preferentially prevents the expression of *survivin* at the protein level. The effects of YM155 have been investigated as a treatment in isolation and in combination with various other chemo- and radio- therapeutic regimens (see the review in [43]). In particular, Iwasa et al. [27] demonstrated that YM155 induced *survivin* suppression markedly enhanced the effects of radiation on tumor growth (for further details, see Section 3).

1.2 Mathematical Modeling of Cancer Stem Cells

Notwithstanding the incredible amount of research done into the role of CSCs in disease progression and treatment, much remains unknown. In attempts to explore these dynamics, numerous mathematical models have been developed and analyzed, employing various mathematical techniques from spatially homogeneous ordinary differential equation (ODE) models [26] and spatially-dependent integro-differential equation (iDE) models [10,26] to computational and *in-silico* models [42], and combinations thereof [48], among others. These mathematical results have supported and informed further biological investigations in many aspects of cancer biology. In particular, the models first proposed by Hillen et al. in [26] have been investigated rigourously with focus on both the mathematical sides [10, 26, 37] and biological sides [7].

The phenomenon of dedifferentiation has been described mathematically in a number of ways, including Markov state transition models providing evidence for spontaneous *in-vivo* dedifferentiation in breast cancer [22], *in-silico* models investigating tumor heterogeneity [48], and morphology [42], and a discrete time compartmental model used to predict optimized radiation schedules [35].

Mathematical models have also been used to evaluate the effectiveness of radiosensitizing strategies. Two such strategies are of particular interest in the context of the CSC model of cancer - differentiation therapy and dedifferentiation therapy. While these two approaches differ in their methods, the desired results are the same: reduce the radioresistant CSC population in order to sensitize the tumor to radiation therapy. While dedifferentiation therapy has yet to be seriously investigated mathematically, differentiation therapy has been modelled by several authors, with the resulting work leading to a number of important findings. In [53] the authors showed that combination differentiation-radiation therapy could control tumors that either modality applied in isolation would fail to control. The authors of [7] echoed these results after applying similar methods to the specific cases of head and neck cancers, metastatic brain cancers and breast cancer. Finally, Konstorum et al. [31] employ the ecological concept of an

"Allee effect" in order to provide an explanation for the effectiveness of a combination of differentiation and radiation therapy.

1.3 Outline

In Section 2 we develop a system of ODEs to model the dynamics between CSCs, NSCCs, and *survivin*. We use two variants of the model; one that assumes a constant rate of dedifferentiation (CD-model) and the other incorporating a *survivin*-dependent rate of dedifferentiation (SDD-model). In Section 3 we fit the models to the data of Iwasa et al. [27]. Using AICc we find that the model incorporating a *survivin*-dependent rate of dedifferentiation offers a better explanation of the data. As in Iwasa we find that a combination of radiation treatment with *survivin* inhibition can significantly increase treatment success. We estimate the gain of combination therapy as compared to the other treatments using the so called *enhancement factor* [27]. In Section 4 we use the fitted model to investigate scenarios that were not considered experimentally. We investigate the timing of radiation treatment schedules as related to the timing of the YM155 administration. We find a dichotomy between different effects. Since YM155 increases the tumor's radiosensitivity, it might be useful to either hit the tumor at the beginning with a large dose to keep it small, or, to wait for a few days after the start of YM155 therapy and irradiate the more sensitive tumor after some delay. The optimal schedule depends on the total amount of radiation used. We close with a discussion in Section 5.

2 The CSC-*survivin* Model

Our model expands on work first presented by Hillen et al. in [26] by incorporating *survivin* and dedifferentiation into their simplified ODE model. For sake of clarity, we recall the original ODE model of [26] here, which reads:

$$\begin{aligned} \frac{du(t)}{dt} &= \underbrace{\delta\gamma_s k(p)u}_{\text{growth of CSC pop.}} \\ \frac{dv(t)}{dt} &= \underbrace{(1-\delta)\gamma_s k(p)u}_{\text{differentiating division of CSC}} + \underbrace{\gamma_d k(p)v}_{\text{growth}} - \underbrace{\tau_d v}_{\text{death}} \end{aligned} \tag{1}$$

where $u(t)$ and $v(t)$ are the CSC and NSCC densities at time t, respectively. To explain the first terms on the right hand side of (1), we consider the following argument for constant mitosis rate γ. Figure 1 shows the CSC mitosis pathways with probability a for symmetric division into two CSCs, probability b for symmetric commitment into two NSCCs, and probability c for asymmetric division. These probabilities are non-negative and they add to one, $a + b + c = 1$. A corresponding mathematical model

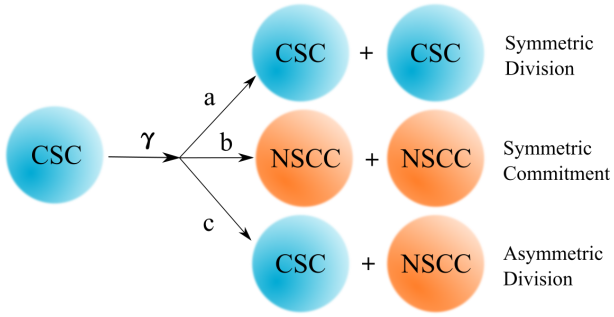

Figure 1: The basic stem cell division model. CSCs can undergo symmetric or asymmetric division, with fractions a for symmetric division, fraction b for symmetric commitment, and fraction c for asymmetric division. γ denotes the mitosis rate. Figure based on that found in [26].

reads

$$\begin{aligned} \dot{u} &= a\gamma u - b\gamma u \\ \dot{v} &= c\gamma u + 2b\gamma u. \end{aligned}$$

Since $a + b + c = 1$, we can replace a and obtain an equivalent system

$$\begin{aligned} \dot{u} &= (1 - c - 2b)\gamma u \\ \dot{v} &= (c + 2b)\gamma u. \end{aligned} \tag{2}$$

If we now choose $\delta := 1 - c - 2b$, we observe the equivalent system

$$\begin{aligned} \dot{u} &= \delta\gamma u \\ \dot{v} &= (1 - \delta)\gamma u. \end{aligned} \tag{3}$$

Then δ denotes the fraction of daughter cells of CSCs that are CSCs as well and $(1-\delta)$ denotes the fraction of daughter cells of CSCs that are NSCCs.

In (1) we assume that the mitosis rate of CSCs is γ_s, and for NSCC γ_d. The death rate for CSC in the model of [26] is 0 while the NSCC die at a rate of τ_d. Proliferation is tempered in both compartments by a volume constraint - $k(p)$ - which is a decreasing function of the total tumor population p and models the decrease in space available to dividing cells as the population approaches saturation. A schematic of this model (1) is shown in Figure 2 including CSC and NSCC, using only those connections that are indicated by a solid arrow.

In order to elucidate the roles of *survivin* and dedifferentiation on tumor growth dynamics and radiotherapies, we extend the model (1) by introducing a third compartment, $s(t)$, representing the *survivin* concentration in the tumor environment at time t. Based on the results discussed in the previous sections, we assume that CSCs preferentially express *survivin* at a rate, ω_s, greater than that of NSCCs, ω_d, and that it is released into the tumor environment upon apoptosis. We also assume a positive

decay rate, $\sigma > 0$, reflecting *survivin*'s short lifespan [5]. To reflect *survivin*'s role as inhibitor of apopotosis (IAP), we replace the NSCC death rate, τ_d, from (1) with a decreasing function of the *survivin* concentration, $\tau_d(s)$, such that it reaches maximum at $s = 0$ and approaches it's minimum value as $s \to \infty$. We introduce a function, $\tau_s(s)$ with identical properties to model the CSC death rate as a function of *survivin* levels.

Furthermore, we introduce an increasing function of the *survivin* levels, $\mu(s)$, to model the rate of dedifferentiation. We assume that this rate of dedifferentiation, $\mu(s)$, reaches a minimum value when there is no *survivin* present ($s = 0$), and approaches a maximum value as $s \to \infty$. Note that these assumptions still allow for a constant rate of dedifferentiation.

Combining all of these factors, we arrive at our full CSC-*survivin* model:

$$\begin{aligned}
\frac{du}{dt} &= \underbrace{\delta\gamma_s k(p)u}_{\text{growth of CSC pop.}} + \underbrace{\mu(s)v}_{\text{de-differentiation}} - \underbrace{\tau_s(s)u}_{\text{death}} \\
\frac{dv}{dt} &= \underbrace{(1-\delta)\gamma_s k(p)u}_{\text{differentiating division of CSC}} + \underbrace{\gamma_d k(p)v}_{\text{growth}} - \underbrace{\mu(s)v}_{\text{de-differentiation}} - \underbrace{\tau_d(s)v}_{\text{death}} \\
\frac{ds}{dt} &= \underbrace{\omega_d\tau_d(s)v}_{\text{release by NSCC}} + \underbrace{\omega_s\tau_s(s)u}_{\text{release by CSC}} - \underbrace{\sigma s.}_{\text{decay}}
\end{aligned} \tag{4}$$

A schematic of this model is shown in Figure 2 including the CSC, NSCC and survivin nodes. The final ingredient, the YM155 treatment, will be modelled by making the survivin production rates $\omega_d(y), \omega_s(y)$ dependent of an YM155 concentration $y(t)$, see Section 2.4.

2.1 Functional Forms Used in Numerical Simulations

While the assumptions made on the remaining functional coefficients - volume constraint, $k(p)$, rate of dedifferentiation, $\mu(s)$, and rates of CSC and NSCC death, $\tau_s(s)$, and $\tau_d(s)$ respectively - are sufficient for mathematical analysis, in order to obtain numerical results we must choose specific functional forms.

For the volume filling constraint $k(p)$ we use a functional form that was introduced in Wang [51]. It allows to account for the elastic properties of cells, as they are deformable, and can squeeze into openings. Solid objects would have a volume constraint of $k(p) = 1 - p$, however, deformable objects are better described by other exponents, for example

$$k(p) = 1 - p^4, \tag{5}$$

as has been used in [26, 51]. We parameterize the rate of dedifferentiation, $\mu(s)$, as a sigmoid curve with three parameters - minimum, μ_{min}, and maximum, μ_{max}, rates together with a *survivin* level, s_{mid}, at which the rate of dedifferentiation is half the

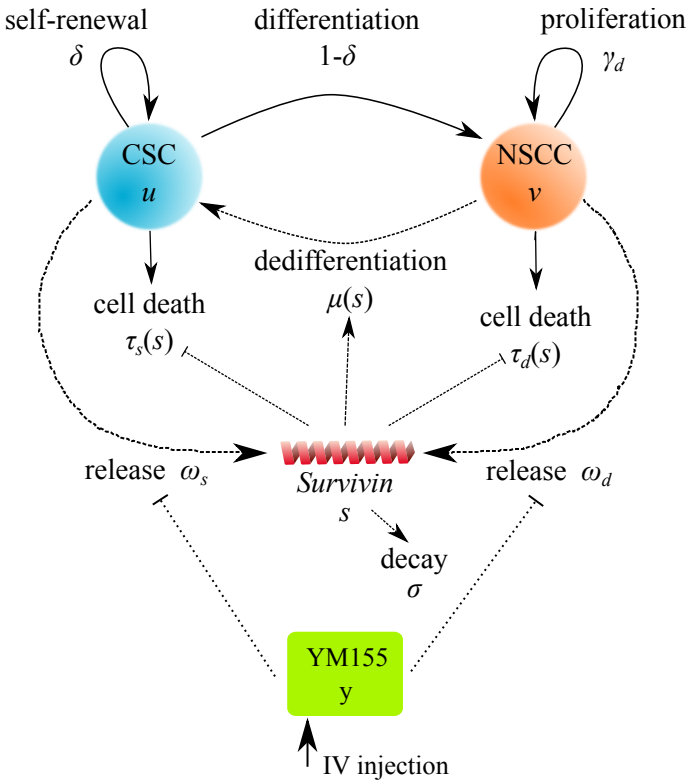

Figure 2: Cartoon of the mathematical model. Solid arrows indicate relationships included in the original model of Hillen et al. [26], and the dashed arrows denote the relationships added here.

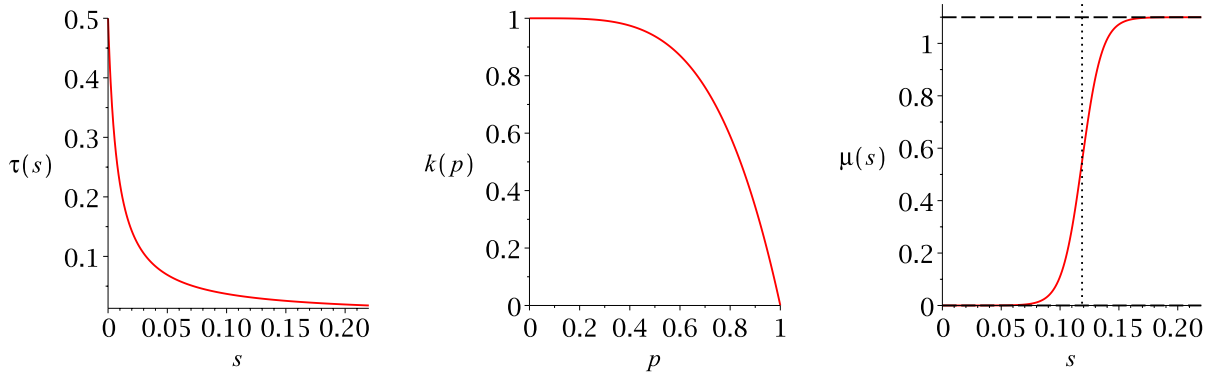

Figure 3: Functional forms used in the numerical simulations. Left: death rate as a function of *survivin* concentration as in (7) with $\tau_{max} = 0.5$, $\tau_{min} = 0$, and $\theta = 125$. Middle: volume filling constraint as in (5). Right: rate of dedifferentiation as a function of *survivin* concentration as in (6), with $\mu_{max} = 1.0997$ (upper dashed), $\mu_{min} = 10^{-6}$ (lower dashed), and $s_{mid} = 0.1187$ (dotted).

maximum rate. Specifically, we employ the functional form

$$\mu(s) = \frac{\mu_{max}}{1 + \left(\frac{\mu_{max} - \mu_{min}}{\mu_{min}}\right)^{1 - \frac{s}{s_{mid}}}} \tag{6}$$

where $\mu_{max} > 2\mu_{min} > 0$ (see Figure 3). As for the death rates, $\tau_s(s)$ and $\tau_d(s)$, we use a maximum, $\tau_{s,max}$ and $\tau_{d,max}$, and a minimum, $\tau_{s,max}$ and $\tau_{d,max}$, rate of cell death for CSCs and NSCCs respectively, together with sensitivity parameters, θ_s and θ_d, to model the rate of cell death as a function of *survivin* levels. Specifically, we employ the functional form

$$\tau_s(s) = \tau_{s,min} + (\tau_{s,max} - \tau_{s,min}) \left(\frac{1}{1 + \theta_s s}\right) \tag{7}$$

for the CSC death rate (and for NSCC, simply replace the subscript s's in the above with d's). For simplicity, we assume throughout that $\tau_{s,min} = \tau_{d,min} = 0$. Representative plots of these functions are given in Figure 3.

2.2 Modeling Radiation

To model the effects of radiation therapy on the tumor population, we employ a rather simple version of the linear-quadratic (LQ) model [28]. The mathematical modeling of radiation effects on tissues is a lively and active field of research and many advanced models are discussed (see e.g. [14,19,21,25]). The LQ model, although simplistic, has proven to be a useful tool in many applications and in clinical practice. In our case, the LQ model allows for a very good fit of the model to the data of Iwasa.

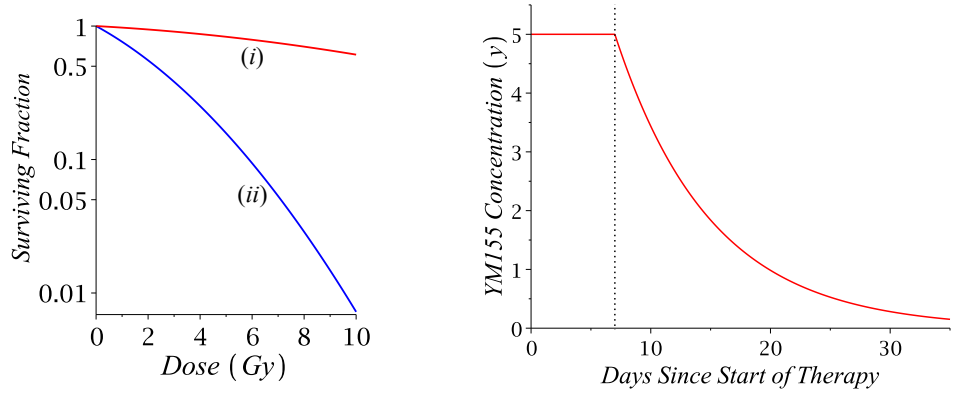

Figure 4: Left: Surviving fraction as a function of radiation dose as prescribed by the LQ model. (i) Surviving fraction of radioresistant CSCs, and (ii) that of the radiosensitive NSCCs, with LQ parameters related according to (10). Right: Modeling YM155 treatment. YM155 concentration as a function of time as in (12). Treatment begins at day 0 and terminates on day 7 (marked with dotted line). For parameter values used, see Table 1.

The standard LQ model assumes homogeneous tumor radiosensitivity, and for a given dose, d, prescribes a surviving fraction according to the relation

$$S(d) = \exp(-\alpha d - \beta d^2), \tag{8}$$

where α (Gy^{-1}) and β (Gy^{-2}) represent cell killing as a result of single and double hit events, respectively [4]. These parameters are tissue-specific and their ratio - α/β - can be determined experimentally. (For the specific case of NSCLC an α/β ratio of $10Gy$ has been widely used [1, 19, 29, 46].) Several attempts have been made to incorporate the observed radiosensitivity heterogeneity into the LQ model, ranging from simply setting $\beta = 0$ for the CSCs [7], to assuming a fixed fraction, q, of CSCs and modifying the surviving fraction function in (8) to read

$$\tilde{S}(d) = q\exp(-\alpha_s d - \beta_s d^2) + (1-q)\exp(-\alpha_d d - \beta_d d^2), \tag{9}$$

where α_s, β_s are LQ parameters specifically for CSCs, and α_d, β_d are LQ parameters specifically for NSCCs [54]. In [35] a constant, $\chi \in (0, 1]$ is used to relate the CSC LQ parameters to the NSCC LQ parameters via the relation

$$\alpha_s = \chi\alpha_d, \text{ and } \beta_s = \chi\beta_d. \tag{10}$$

Here we use this simple method (10) from [35] and assume throughout that $\chi = 0.1$. The surviving fractions for CSC and NSCC as function of dose d are shown on the left of Figure 4.

Beyond the cell killing prescribed by the LQ model, we incorporate the observed increase in *survivin* levels in response to radiation. Assuming that this release is related to cell death, we assume that the amount of *survivin* released in response to radiation is proportional to the population of cells that have been killed by radiation.

2.3 Implementation

As for the implementation of this modified LQ model, we adopt a typical approach for the analysis of impulsive differential equations, while assuming that the direct effects of radiation are instantaneous. The specific implementation procedure is as follows:

1. Run the simulation until the first dose of radiation is to be administered (at time t^* say).

2. Determine surviving fractions of the CSC and NSCC populations according to the LQ model, using the CSC and NSCC specific LQ parameters as outlined in (10).

3. Adjust the *survivin* levels according the relation

$$s_{post} = s_{pre} + \zeta_s u_{killed} + \zeta_d v_{killed} \tag{11}$$

   where u_{killed} and v_{killed} are determined by the LQ model, ζ_s and ζ_d are constants of proportionality, and $s_{pre,post}$ are the *survivin* levels immediately before and after application of radiation respectively.

4. Restart the simulation, using these newly determined values as initial conditions at time t^*.

5. Repeat for the remaining scheduled doses of radiation.

2.4 Modeling *Survivin*-Inhibition with YM155

To model the *survivin* inhibiting effect of YM155, we introduce the function $y(t)$ to denote the concentration of the drug within the tumor region at time t. Specifically, we assume the following drug concentration dynamics:

$$y(t) = \begin{cases} \tilde{d} & : \text{during treatment} \\ c\exp(-a(t-b)) & : \text{else,} \end{cases} \tag{12}$$

where the parameters a, b, c, d will be defined below. A plot of this function is provided on the right of Figure 4. This specific functional form is chosen to reflect a number of important biological factors. First, the application of YM155 is done via continuous IV infusion. Therefore, in a well vascularized tumor the drug concentration will rapidly reach saturation and remain saturated until the end of drug administration. For this reason, we have chosen to assume that the YM155 levels are constant throughout the course of treatment administration. Once treatment has stopped, the YM155 concentration will quickly decrease as the drug decays and diffuses away from the tumor region. This decay is modelled as a simple exponential decay. In order for the function $y(t)$ to be continuous at the end of treatment, we choose

$$b = \frac{\ln\left(\frac{\tilde{d}}{c}\right)}{a} + T \tag{13}$$

where T denotes the time (days) over which treatment is administered.

With the values of $\tilde{d}$ and T determined by the data from [27] (see Section 3 and Table 1), and b as above, we are left to determine the values of a and c. To do this, we consulted data from the references within [43], which demonstrated that YM155 remained effective in tumor suppression or regression for approximately a week after the conclusion of drug administration. Using this information, we chose the parameters a and c in such a way that the YM155 concentration decayed to approximately 50% saturation one week after the end of treatment. The specific parameter values determined are presented in Table 1 and the specific functional form used in what follows is presented on the right of Figure 4.

Now that we have the YM155 levels as a function of time, $y(t)$, we incorporate this into our model in such a way that higher levels of YM155 result in lower production rates of *survivin*. This is done by replacing the constant *survivin* production rates, ω_s and ω_d, in the full model (4) with decreasing functions of the YM155 levels, $y(t)$. Much as we did for the *survivin*-dependent death rates (7), we use the functional form

$$\omega_s(y) = \omega_{s,min} + (\omega_{s,max} - \omega_{s,min}) \left(\frac{1}{1 + \psi_s y} \right) \tag{14}$$

that achieves a maximum rate of *survivin* production, $\omega_{s,max}$, when there is no YM155 present in the tumor environment, $y = 0$, and approaches a minimum rate, $\omega_{s,min}$, as $y \to \infty$. As with the death rates (7), this also incorporates a sensitivity parameter, ψ_s. While the above form (14) is for the CSC *survivin* production rate, the same form is employed for NSCC *survivin* production, with the subscript s's replaced with d's. For simplicity, we assume throughout that $\omega_{s,min} = \omega_{d,min} = 0$.

3 Results

In order to investigate the role of *survivin* and dedifferentiation in radioresistance, we fit two versions of our model (4). The first version incorporates a constant, *survivin*-indepenedent rate of dedifferentiation while the second version incorporates the *survivin*-dependent rate of dedifferentiation highlighted in (6). These models are chosen in order to determine whether or not *survivin*-dependent dedifferentiation can provide an explanation for the observed radiosensitizing effect of *survivin* inhibition. For simplicity, we introduce the abbreviations CD and SDD to refer to the constant dedifferentiation and *survivin* dependent dedifferentiation models respectively.

In what follows, we fit our full model (4) to data from the NSCLC cell line H460 [27]. In their study of the radiosensitizing effect of YM155, Iwasa et al. [27] observed the growth of NSCLC cells in nude mice under four distinct treatment regimens:

(i) a control treatment, in which the tumor was allowed to grow without interference,

(ii) a γ-radiation treatment, in which $10Gy$ of radiation was administered in $2Gy$ fractions each day over the course of 5 days,

(iii) a YM155 treatment, in which the small-molecule *survivin* inhibitor YM155 was administered by continuous IV infusion over the course of 7 days with a dose of 5 mg/kg, and

(iv) a combination therapy, which combines the previous treatment modalities (ii) and (iii), with the YM155 treatment beginning on day 0 and the radiation beginning on day 3.

The tumor volumes were measured over the course of treatment for 8 mice per treatment group, and the data is presented as means (dots) and standard errors (bars) in Figure 5. Here we have assumed that Iwasa et al. [27] stopped data collection as the tumor approached volume saturation. We normalized this maximum tumor volume to correspond to a fractional tumor burden of 1, and we used our model to fit the normalized data following the procedures outlined in the following section. Throughout, we assume the tumors at the beginning of treatment are dominated by the radiosensitive NSCCs ($v(0) = 0.05$, and $u(0) = 0.0025$), and that the initial *survivin* concentration is very low ($s(0) = 0.0004$) - representative of newly formed tumors.

3.1 Fit to Control Data

First, the total tumor population, $p = u+v$, as determined by our model (4) is fit to the control data (i) from [27] using MATLAB's 'nlinfit' together with the 'ode45' solver. Throughout, we have fixed the fraction of symmetric CSC divisions at $\delta = 0.01$ [7, 26] and the minimum rate of dedifferentiation at $\mu_{min} = 10^{-6}$. In order to simplify the optimization process, we optimized at most 4 parameters at a time, fixing the remaining values with biologically relevant values. For example, the *sensitivity* parameters (θ's and ψ's) together with the max death rates ($\tau_{s,max}$ and $\tau_{d,max}$), *survivin* decay rate, σ, and *survivin* production rates, ω_s and ω_d, may be fixed and the remaining parameters (CSC/NSCC mitosis rates - γ_s and γ_d - max rate of dedifferentiation, μ_{max}, and the *survivin* level at which the rate of dedifferentiation is half its maximum rate, s_{mid}) optimized. This process was then repeated for a wide array of fixed parameter values. Once a best fit was obtained, the optimized parameter values were then fixed, and the previously fixed parameters optimized following the same process as described above. This process was repeated until the changes in the residual sum of squares (RSS) were no longer significant. Finally, because we fixed $\delta = 0.01$ throughout, the $AICc$ values were then calculated using a number of parameters of $K = 10$ (CD model) and $K = 12$ (SDD model).

Table 1: Parameter Values Used

Parameter	CD model	SDD model
Initial Conditions		
$u(0)$ - Initial CSC density	0.0025	0.0025
$v(0)$ - Initial NSCC density	0.05	0.05
$s(0)$ - Initial *survivin* concentration	0.0004	0.0004
Control Parameters		
δ - Fraction of CSC after mitosis of CSC	0.01	0.01
$\gamma_s(time^{-1})$ - CSC mitosis rate	0.0506	0.0659
$\gamma_d(time^{-1})$ - NSCC mitosis rate	2.18	0.6256
$\tau_{s,max}(time^{-1})$ - Max CSC death rate	0.027	0.002
$\tau_{d,max}(time^{-1})$ - Max NSCC death rate	0.4377	0.5
$\mu_{max}(time^{-1})$ - Max rate of dedifferentiation	3.0806	1.0997
$\omega_{s,max}(time^{-1})$ - Max CSC *survivin* release	99.47	77
$\omega_{d,max}(time^{-1})$ -Max NSCC *survivin* release	4.5376	55
$\sigma(time^{-1})$ - *Survivin* decay rate	0.475	0.475
$\theta_s(concentration^{-1})$ - CSC *survivin* sensitivity	7.75	250
$\theta_d(concentration^{-1})$ - NSCC *survivin* sensitivity	20.9754	125
$\mu_{min}(time^{-1})$ - Min rate of dedifferentiation	-	0.000001
$s_{mid}(concentration)$ - $\frac{\mu_{max}}{2}$ *Survivin* concentration	-	0.1187
Radiation Parameters		
α/β (Gy) - Tissue specific LQ parameter	10	10
χ - constant relating CSC and NSCC LQ parameters	0.1	0.1
$\alpha_s(Gy^{-1})$ - CSC DNA damage single tract	0.038	0.02465
$\alpha_d(Gy^{-1})$ - NSCC DNA damage single tract	0.38	0.2465
$\beta_s(Gy^{-2})$ - CSC DNA damage double tract	0.0038	0.002465
$\beta_d(Gy^{-2})$ - NSCC DNA damage double tract	0.038	0.02465
ζ_s - CSC *survivin* release constant	1.0	3.6
ζ_d - NSCC *survivin* release constant	0.01	0.05
YM155 Parameters		
$\tilde{d}$ (mg/kg) - YM155 dose	5	5
$a(time^{-1})$ - YM155 decay rate	0.125	0.125
b $(time)$ - Time to concentration of c mg/kg	19.876	19.876
c (mg/kg) - YM155 concentration at time $t = b$	1	1
T $(time)$ - Length of treatment	7	7
ψ_s (kg/mg) - CSC YM155 sensitivity	12	17.75
ψ_d (kg/mg) - NSCC YM155 sensitivity	8025	12904

We also note that any optimized parameter values that did not make sense biologically (ex: negative parameters) were rejected. Because biologically relevant values for the *sensitivity* parameters are unknown, the only restriction on these parameters was that they be non-negative. The fit parameters for both versions of the model are presented in Table 1.

3.2 Fit to Treatment Data

Once our model was calibrated to fit the control data from [27], the radiation treatment procedure (ii) was applied to the calibrated model and fit to the radiation

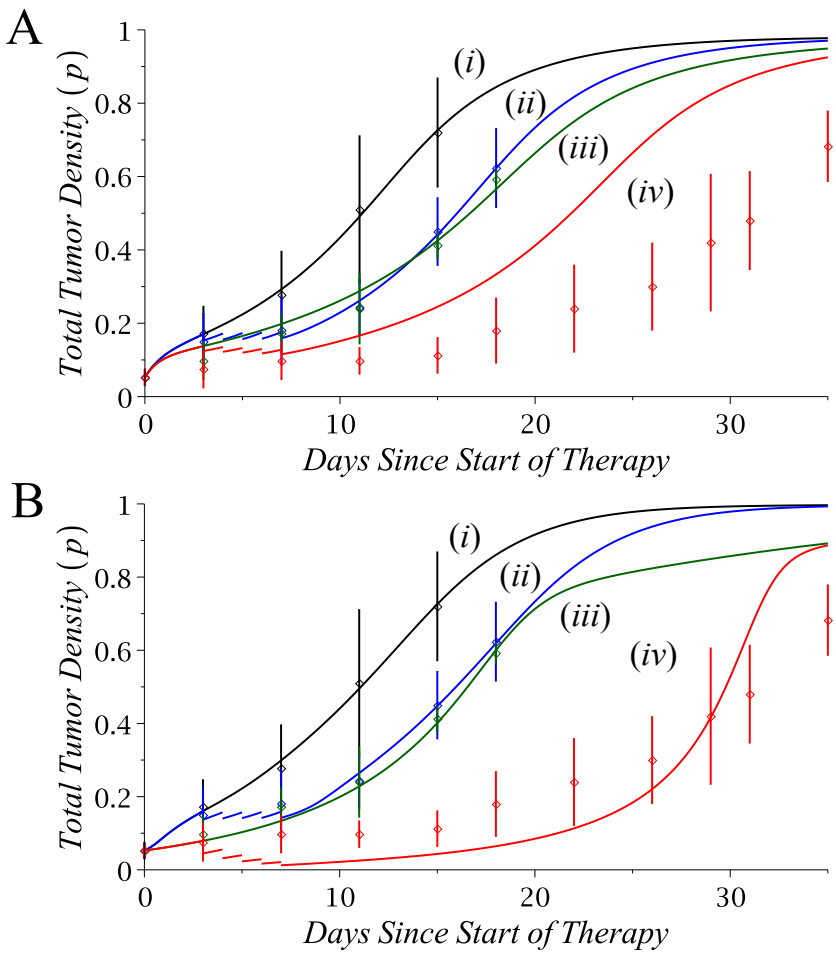

Figure 5: Comparison of two models of dedifferentiation. A: Constant dedifferentiation (CD-model) and B: *survivin*-dependent dedifferentiation (SDD-model). Parameters are as in Table 1. Data points are from [27] and the curves are model predicted tumor densities, $p = u + v$. Treatment groups are indicated as follows: (i) Control, (ii) Radiation, (iii) YM155, and (iv) Combination.

data from [27]. A radiation treatment fit was obtained by manipulating ONLY the 6 radiation-specific parameters - specifically the LQ parameters, $\alpha_{s,d}$ and $\beta_{s,d}$, and the *survivin* release constants, $\zeta_{s,d}$. As before, this optimization process was done until the changes in RSS were negligible, and the $AICc$ values were determined using $K = 16$ and $K = 18$ for the CD and SDD models respectively. The radiation-associated parameters used in our results are listed in Table 1 under the heading of 'Radiation Parameters'.

A similar process was undertaken to fit the YM155 data (iii) from [27]. Starting with the model (4) calibrated to the control data, we replaced the constant rates of *survivin* production with the decreasing functions of YM155 levels defined in (14) (with the maximum production rates coming from the control calibration). The 2 sensitivity parameters, ψ_s and ψ_d were then manipulated to fit the model to the YM155 data. $AICc$ values were determined using $K = 12$ and $K = 14$ for the CD and SDD models respectively. All of the parameters associated with YM155 treatment are listed in Table 1.

While the original fitting of the control data was done using MATLAB, the remainder of the process was done using MAPLE and its 'desolve' function.

3.3 Model selection

Finally, once the control and both single treatment modalities (ii) and (iii) have been fit (i.e. all the parameters have been determined) the combination model (iv) is determined. In other words, the combination therapy is not explicitly fit at any point, rather it follows directly from the parameter values obtained from fitting (ii) and (iii). To determine which of the model variants - CD or SDD - best fits the data, we use the small data corrected Akaike Information Criterion ($AICc$) which has become widely used in multimodel selection [11]. Letting RSS denote the residual sum of squares, the $AICc$ is given by

$$AICc = n \ln\left(\frac{RSS}{n}\right) + \frac{2Kn}{n - K - 1} \tag{15}$$

where n denotes the number of observed data points and K is the number of estimable parameters in the model. This criterion has the effect of rewarding a model for fitting the observed data well and punishing it for the number of parameters it uses. In general, the model with the lowest $AICc$ value provides the best explanation for the data. It is important to note that $AICc$ values are only meaningful when looking to determine which among a set of candidate models best explains a single data set. In particular, meaningful comparisons of AICc values across data sets cannot be made.

Table 2 reports our RSS and $AICc$ values for the two candidate models across the four distinct treatment data sets, with the lowest $AICc$ value in each treatment modality bolded. Our results show that the CD model provides the best explanation for the control and radiation data, while the SDD model best explains the YM155 and combination treatments. The two extra parameters in the SDD model are the reason for the model's higher $AICc$ values in the control and radiation data, with

Table 2: RSS and AICc values for the CD and SDD models for the four treatment regimens examined. Values representing best explanation for the data under each treatment modality are bolded. The difference (Δ) in the AICc values is shown in the last column.

	Treatment	CD RSS	SDD RSS	CD AICc	SDD AICc	Δ
(i)	Control	0.000645	0.000875	**-61.448**	-58.256	3.192
(ii)	Radiation Only	0.000826	0.00106	**-70.798**	-68.467	2.331
(iii)	YM155 Only	0.00545	0.00215	-62.599	**-66.285**	3.686
(iv)	Combination	0.667	0.124	-80.339	**-93.321**	12.982

the RSS values within the same order of magnitude for all treatments other than the combination data, in which the SDD RSS is markedly lower, resulting in a significantly superior AICc value.

More important than the raw $AICc$ values are the differences in $AICc$ values between candidate models, Δ. While the Δ value is relatively small for the control, radiation, and YM155 treatments, it is large for the combination data, suggesting that the SDD model explains the combination data significantly better than the CD model does.

The results in Table 2 are confirmed visually in Figure 5, which shows the total tumor densities, $p = u + v$, fit to Iwasa et al.'s data [27] using the CD model (top) and the SDD model (bottom). Iwasa et al.'s data are represented by points (means) and bars (standard error), and our model predictions are the curves. Control data and predictions are in black (i), radiation is in blue (ii), YM155 in green (iii), and combination is in red (iv) (Color version online).

3.4 Growth Delay and Enhancement Factor

As a third measure to discriminate between the models, we quantify the enhanced effect of radiation when applied in combination with YM155, as compared to when applied in isolation. We quantify the difference in those treatments by the growth delay and an enhancement factor as introduced in [27]. Let T_x denote the time at which the total tumor density reaches five times the initial density (this endpoint was chosen to coincide with that used in [27]) under treatment $x \in \{(i), (ii), (iii), (iv)\}$. In other words, T_x satisfies

$$p(T_x) = 5p(0) = 5p_0. \tag{16}$$

Next, for treatment $x \in \{(ii), (iii), (iv)\}$ define the tumor growth delay under this treatment, GD_x, to be the difference

$$GD_x = T_x - T_{(i)}. \tag{17}$$

Finally, in the combination therapy, growth delay comes as a result of the effect of both YM155 and radiation. We want to determine the portion of this delay that

can be attributed to the radiation component of treatment. In order to do this, we assume that the delay effect of YM155 is the same whether applied in isolation or in combination. Under this assumption, we can determine the tumor growth delay of the combination therapy that is contributable to radiation by computing the difference

$$\text{Combination growth delay contributable to radiaiton} = GD_{(iv)} - GD_{(iii)}. \tag{18}$$

This value is then used to determine the 'enhancement factor' of radiation used in combination over use in isolation via

$$EF = \frac{GD_{(iv)} - GD_{(iii)}}{GD_{(ii)}}. \tag{19}$$

Table 3: Values used to determine radiation enhancement factors

	Treatment	Time to $p = 0.2625$	Growth Delay	Enhancement Factor
	CD model			
(i)	Control	6.181	-	-
(ii)	Radiation Only	11.026	4.845	-
(iii)	YM155 Only	10.038	3.857	-
(iv)	Combination	15.692	9.511	**1.16**
	SDD model			
(i)	Control	6.100	-	-
(ii)	Radiation Only	10.951	4.851	-
(iii)	YM155 Only	12.017	5.917	-
(iv)	Combination	26.894	20.794	**3.07**

With an enhancement factor of 1.16 (see Table 3), the CD model predicts only a slight increase in radiation effectiveness when applied in combination. In contrast, the SDD model predicts an enhancement factor of 3.07, very close to the value of 3.0 reported in [27].

3.5 Model Comparison

In order to obtain a deeper understanding of the results outlined above, we take a closer look at the CSC/NSCC dynamics in both the CD and SDD models. In Figure 6, we plot the fraction of NSCCs within the tumor as a function of time in the CD model (left) and the SDD model (right). Because of the relative radioresistance of CSCs compared to NSCCs, we can view this fraction as a simple measure of the tumor's radiosensitivity. Indeed, the larger the fraction of NSCCs within the tumor, the more radiosensitive the tumor (and vice-versa). Therefore, we view the plots in Figure 6 as the tumor's sensitivity to radiation as a function of time. With this view in mind, we make some observations.

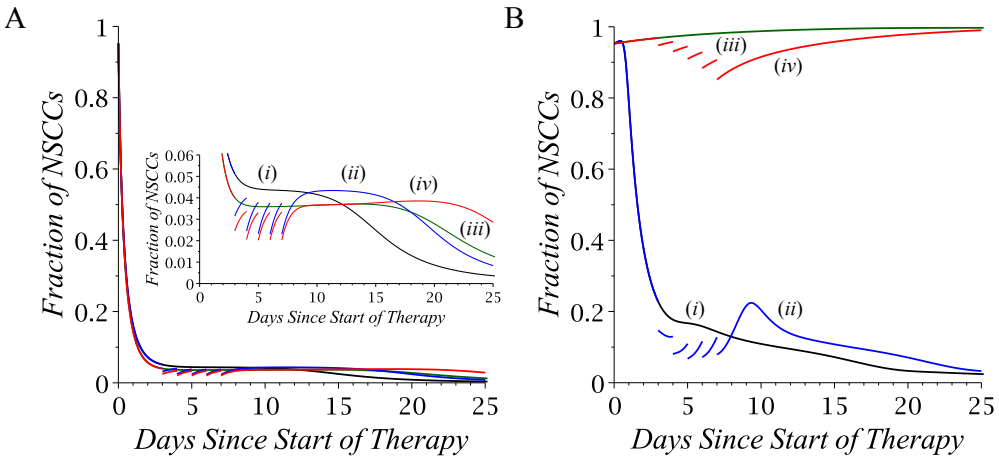

Figure 6: Radiosensitivity plots. Fraction of NSCCs as proportion of total tumor population as a function of time. In both plots, treatments are indicated by: (i) Control, (ii) Radiation, (iii) YM155, and (iv) Combination. (A) Constant dedifferentiation model. Inset is a zoom of the full plot in order to better illustrate the dynamics (note difference in scales). (B) Full, *survivin*-dependent dedifferentiation model.

The CD model - regardless of treatment modality - predicts tumors that quickly become dominated by radioresistant CSCs. In particular, because the rate of dedifferentiation is *survivin* independent, the YM155 does nothing to promote radiosensitivity, thereby explaining the low enhancement factor determined in the previous section. In contrast, the SDD model shows a clear demarkation between the treatments that do and do not inhibit *survivin*. Indeed, with a *survivin* dependent rate of dedifferentiation, the *survivin* inhibiting effects of YM155 include decreased - almost non-existent - rates of dedifferentiation (see Figure 7). As a result, treatments incorporating YM155 lead to dramatically more radiosensitive tumors, and it is this increased radiosensitivity that is responsible for the predicted enhancement factor of 3.07.

4 Other Fractionation Schedules

Using the calibrated SDD model, we investigate the effects of different radiation fractionation and scheduling on tumor growth. For simplicity we test a number of simple fractionation schedules, the details of which are outlined in Table 4. All schedules are administered over the course of 5 days and consists of a total cumulative radiation dose of $10Gy$. For sake of control, we test these radiation schedules both as a single treatment and in combination with YM155, the results of which are shown in Figure 8, showing the temporal evolution of the total tumor population in response to the various radiation schedules.

As can be seen in Figure 8 and Table 5, when used in isolation, the various radiation schedules vary little in their tumor suppression results, with tumor suppression effects

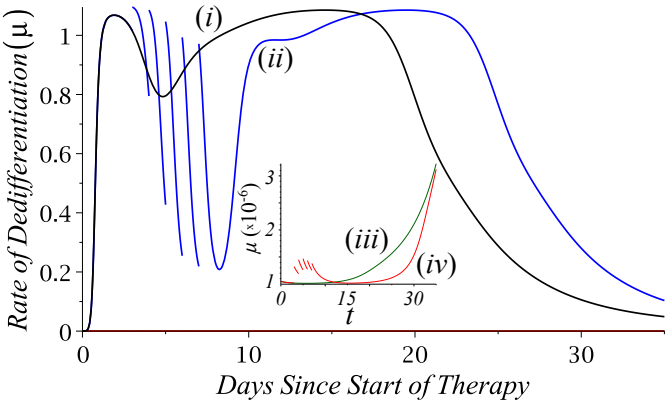

Figure 7: Rates of dedifferentiation as a function of time in the fit *survivin*-dependent dedifferentiation model. Treatment modalities marked as follows: (i) Control, (ii) Radiation, (iii) YM155, (iv) Combination. Inset shows a magnification of the main plot in order to observe the rate of dedifferentiation in the therapies incorporating YM155. Note the difference in scales.

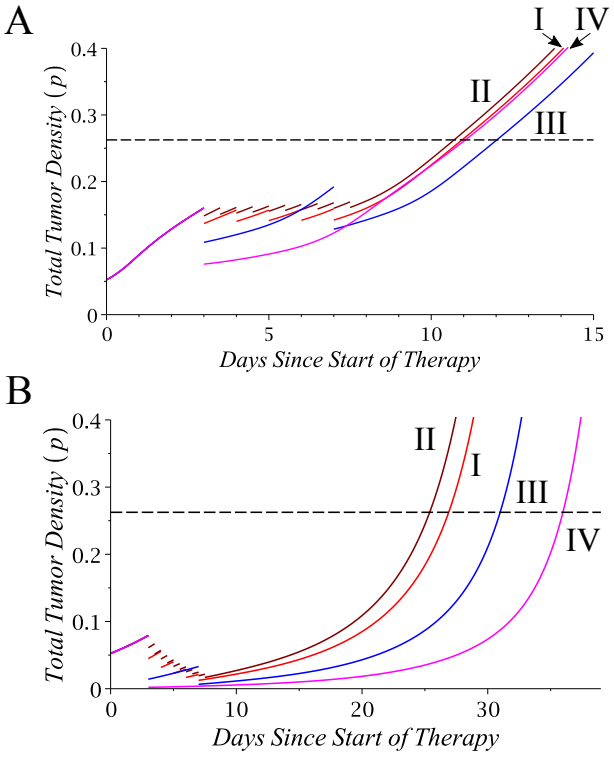

Figure 8: Tumor suppression effect of various radiation schedules. Top: tumor suppression when radiation is applied in isolation. Bottom: tumor suppression when radiation is applied in combination with YM155. Note the different time scales between the two plots. Dashed line denotes the endpoint tumor density of $0.2625 = 5p(0)$. Schedule details are in Table 4 and parameters in Table 1.

Table 4: Radiation Schedules Tested. In our simulations, these five day schedules commence at time $t = 3$ days to coincide with the data from [27]. For all schedules except for the hyperfractionated schedule, doses were administered at the same time each day. For the hyperfractionated schedule, doses were administered 12 hrs apart from each other.

Schedule	Day 1	Day 2	Day 3	Day 4	Day 5
(I) Standard	2 Gy	2 Gy	2 Gy	2 Gy	2 Gy
(II) Hyperfractionated	1 Gy $\times 2$	1 Gy $\times 2$	1 Gy $\times 2$	1 Gy $\times 2$	1 Gy $\times 2$
(III) Hypofractionated	5 Gy	-	-	-	5 Gy
(IV) Single Dose	10 Gy	-	-	-	-

of the best and worst performing schedules differing by just over 1 day. That being said, the best performing schedule in this case is the hypofractionated schedule (III), using two large doses at the begining and ending of the treatment time. By consulting Figure 9 it becomes clear that the hypofractionated schedule (III) is the best performing, because the second dose is applied near a peak of tumor sensitivity.

On the other hand, when these schedules are applied in combination with YM155, there is a marked difference in performances, with the best and worst performing schedules differing in their tumor suppression effects by approximately 10 days (see Table 5). And in contrast to the results when applied in isolation, the best performing schedule when applied in combination, is a single, large dose at the begining of the treatment window (IV), and corresponds to a radiation enhancement factor of 4.84 (see Table 5). This is greater than the value of 3.1 reported in [27], but does mirror their results that single dose had a higher radiation enhancement factor than did standard fractionation. The reason for schedule (IV)'s superior performance in this case can be seen in the NSCC plots in Figure 9, where the single dose takes advantage of the increased tumor sensitivity to radiation, whereas the other schedules include multiple doses with each one being applied on a more resistant tumor, resulting in less effective treatments.

Table 5: Times to $5p_0$ and enhancement factor (19) for the radiation schedules tested using the calibrated SDD model. For details of the schedules, see Table 4. Bolded values denote the best performing schedule in each treatment group.

Radiation Schedule	Radiation Only	Combination	Enhancement Factor
(I) Standard	10.951	26.894	3.07
(II) Hyperfractionated	10.705	25.380	2.90
(III) Hypofractionated	**12.020**	30.985	3.20
(IV) Single Dose	11.053	**35.978**	4.84

We also consider the CSC fraction 1 day after the final application of radiation as was done by Leder et al. [35], the results of which are given in Table 6. While we are

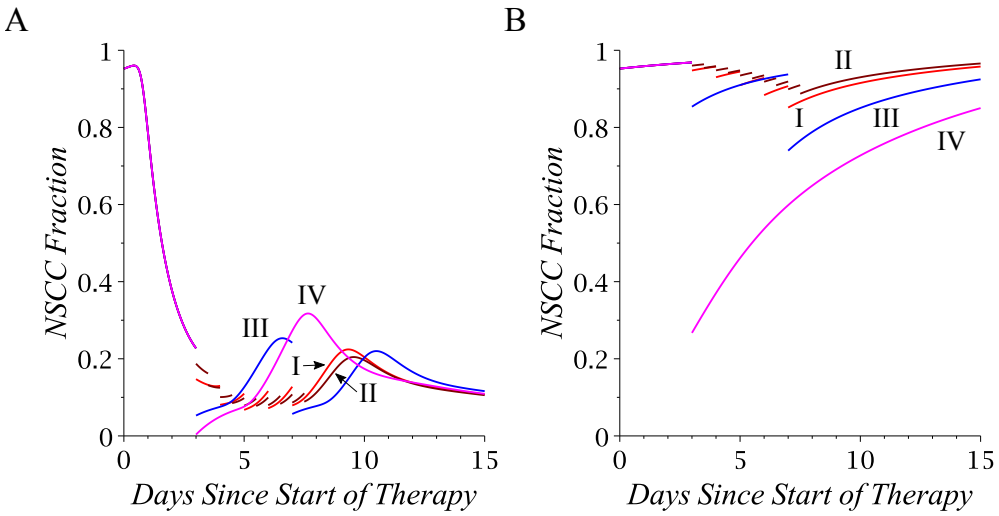

Figure 9: NSCC fractions for various radiation schedules. (A) NSCC fractions when radiation is applied in isolation. (B) NSCC fractions when radiation is applied in combination with YM155. Schedule details can be found in Table 4 and parameters used can be found in Table 1.

able to confirm Leder's findings that the best performing radiation schedule resulted in the highest enrichment of CSC fraction relative to standard frationation when applied in combination, we are unable to confirm these results for schedules applied in isolation. This suggests that factors other than simply CSC enrichment are likely to play a role in determinations of optimized radiation schedules.

Table 6: CSC fractions relative to standard fractionation one day after administration of final dose of radiation for various radiation fractionation schedules.

Radiation Schedule	Radiation Only	Combination
(I) Standard	1	1
(II) Hyperfractionated	0.983	0.759
(III) Hypofractionated	1.066	1.760
(IV) Single Dose	1.098	5.234

4.1 The Timing of Radiation

Based on the observations made in the previous section, that the hypofractionated schedule (III) performed best in isolation because the timing of radiation took advantage of the tumor's radiosensitivity, we turn our investigation toward the interplay between tumor density and tumor sensitivity on the effect of radiation timing. Before we consider treatment timing, we consider tumor densities and NSCC fractions for the control case (i) and for the YM155 treatment case (iii) without any radiation

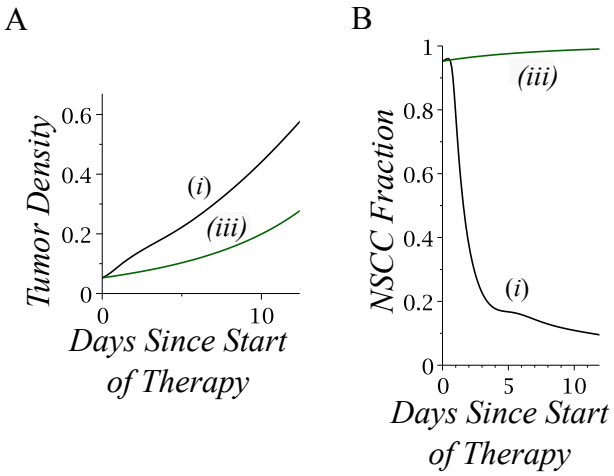

Figure 10: tumor densities (A) and NSCC fractions (B) for control (i) and YM155 treatment (iii). These are details of Figures 5 and 6 and were made using the calibrated SDD model with parameters as in Table 1.

treatment. The corresponding curves are shown in Figure 10. Given these growth characteristics, we consider only single dose schedules, with the dose being applied at different times along these curves. For each $j = 1, \ldots, 48$ we explore the radiation timing at radiation times $t_j = j \cdot 6h$ which are chosen in a distance of 6h, up to 12 days. For each radiation application time t_j, we determine the time $T(t_j)$ it takes the tumor to reach the endpoint of $p(T(t_j)) = 5p_0$. This process gives us the time to endpoint as a function of radiation application times, which can then be compared to tumor density and sensitivity values presented in Figure 10. The results of this investigation are presented in Figure 11 for radiation alone (top) and in combination (bottom) using the calibrated SDD model.

Let us first consider the case of radiation applied in isolation (top row in Figure 11). By consulting the control curves, (i), in Figure 10 we observe that the tumor density is monotonically increasing while the tumor sensitivity decreases quickly after a brief initial sensitization. The combination of increased tumor density and decreased radiosensitivity accounts for the rapid initial drops in radiation effectiveness seen in all 3 dose sizes in Figure 11. After this initial decrease however, there is a brief rebound observed for all 3 dose sizes tested, beginning near day 4. This can be contributed to the abrupt slow down in sensitivity loss observable in Figure 10 (B) that occurs at approximately the same time. The brief rebound reaches an apex that appears to be dose-dependent, and begins to fall again.

Similar non-monotonic behavior can be observed in the case of combination therapy, however there are important differences. First, in contrast to the control case, the YM155 treatment sees the tumor monotonically becoming more sensitive to radiation

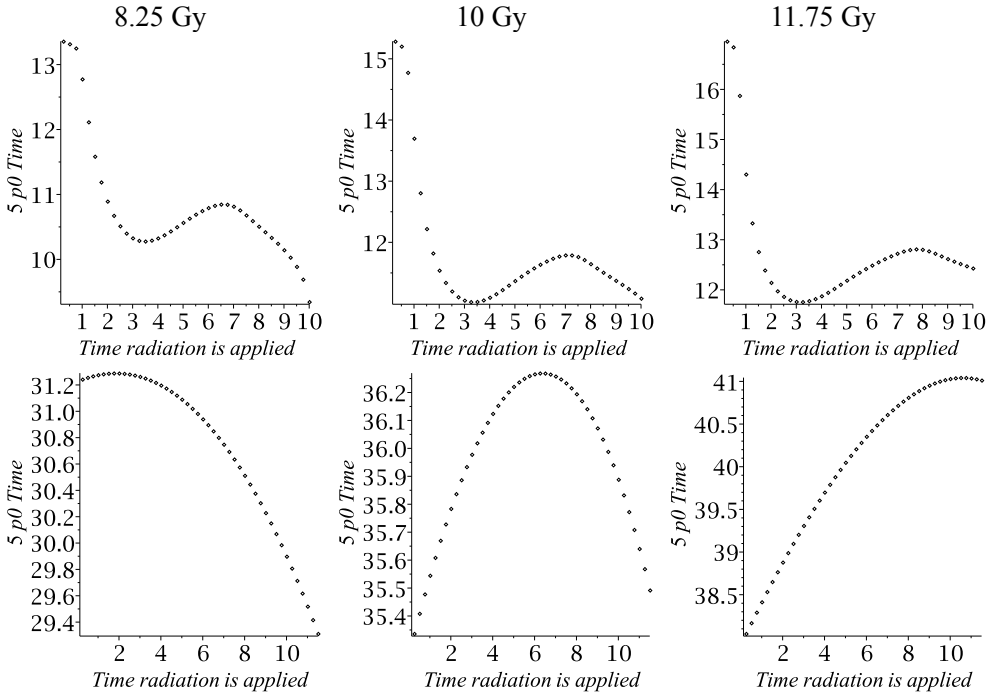

Figure 11: Time $T((t_j))$ at which the tumor density reaches $5p_0$ as a function of radiation application time t_j. Dose sizes are, from left to right, $8.25Gy$, $10Gy$, and $11.75Gy$. Dose sizes shown were chosen in order to best illustrate dose dependence on apex position. The top row shows results when radiation is applied in isolation, and the bottom row shows results when radiation is applied in combination with YM155. All plots were made using the calibrated SDD model with parameters as in Table 1.

(see Figure 10 (B) (iii)). With this being said, for smaller doses our model predicts that the earlier we apply radiation the better, with the benefits of increased sensitivity outweighed by the costs of a larger tumor. This is not the case for larger doses of radiation however. Indeed, in the cases of $10Gy$ and $11.75Gy$ there is a distinct advantage to delay the application of radiation to allow the tumor to become more sensitive to the radiation despite the fact that this delay results in radiation being applied to a larger tumor. This optimum time appears to be dose dependent, with longer delays as we increase the dose size.

5 Discussion

Understanding the underlying mechanisms responsible for radioresistance is crucial in order to develop strategies to enhance the effectiveness of radiation therapies. Under the framework of the CSC hypothesis, we have investigated the role of dedifferentiation and the inhibitor of apoptosis protein *survivin* in the observed radioresistance in NSCLC in mice, using a multicompartmental ODE model. We were able to not only confirm the results of Iwasa et al. [27], but provide a possible explanation for them. The observed radiosensitizing effect of *survivin*-inhibition may come as a result of preventing dedifferentiation, causing a more radiosensitive, NSCC dominated tumor. This result implicates *survivin* in the poorly understood phenomenon of dedifferentiation in CSC driven tumors, and warrants further investigation. Curiously, Rauch et al. [43] report that the radiosensitizing effect of YM155 has only been investigated in [27], the results here suggest further investigation may be worthwhile.

Our results also provide insight into the highly contested question of CSC fractions within CSC driven tumors [17], suggesting that untreated tumors rapidly become dominated by radioresistanct CSCs. This is the case even with an initially NSCC dominated tumor, and is caused by rapidly increasing rates of dedifferentiation in the early stages of tumor growth. Moreover, it is this rapid decrease in radiosensitivity that is ultimately responsible for the predicted radiosensitizing effect of YM155. Indeed, without the pronounced difference in radiosensitivities between the therapies that do and do not include YM155, the enhancement of the effect of radiation would not be as great.

Beyond observed treatment dynamics, our model also provides a glimpse into the poorly understood time dynamics of dedifferentiation. In an untreated tumor, dedifferentiation rates are highly variable, rapidly increasing from it's minimum rate to it's maximum rate in the early stages of tumor development. Soon thereafter, the rate drops slightly, approaches its maximum again and finally drops to a low steady state value. Interestingly, these dynamics mirror those of the NSCC population (see Figure 6) because the *survivin* is released upon cell death, and the death rate among NSCCs is much larger than that among CSCs. These general dynamics are repeated in the radiation therapy, with jumps and dips in response to radiation-induced *survivin* release, and YM155 essentially prevents dedifferentiation according to our model. While

a time-dependent rate of dedifferentiation has been investigated successfully by Leder et al. [35], to the authors' knowledge this is the first time that the time dynamics of dedifferentiation in an untreated tumor have been modelled, but more work is surely needed in order to elucidate the process' role in radioresistance.

Once our model was calibrated to NSCLC data [27], we used it to investigate the role of radiation fractionation scheduling on tumor control. In line with data of [6], the various radiation schedules all performed similarly when applied in isolation. That being said, the best performing schedule when applied in isolation is the hypofractionated schedule, a schedule structure that has been used very effectively for advanced stage NSCLC using stereotactic body radiotherapy (SBRT) [44]. However, this was not the case when the schedules were applied in combination with YM155, where a single, large dose of radiation outperforms standard fractionation by over a week. In comparison, while the hypofractionated schedule also makes use of large doses, the fact that there are two doses in succession means that the second is applied on a more radioresistant tumor than its predecessor. This effect has been documented in a number of cancers [13,20] and proves to be a barricade in determining truly optimized radiation schedules. Indeed, is it more effective to apply radiation to a small tumor or a sensitive tumor? More work needs to be done to determine an optimum balance between the two.

Interestingly, the best performing radiation schedules differed when applied in isolation (hypofractionation) and in combination (single dose). This suggests that optimized radiation schedules determined assuming single treatment therapy, as done in [8, 35], may not be optimum when radiation is applied in combination, further complicating the problem. Further investigation into the mechanisms responsible for this difference in optimum schedules when applied in isolation and in combination are needed. We have also determined that CSC fraction following radiation, tumor density, tumor sensitivity, and dose size all play a role in determining optimized radiation schedules, but more work is needed to elucidate the precise relationships between these factors in order to determine truly optimized radiation fractionation schedules.

While our results are intriguing, cautions must be taken, since a large number of parameters has been fit to a small number of observations. We have attempted to address the issue of local minima in the fitting, by systematically varying our initial parameter estimates over a large domain, and using various metrics for validation. Nevertheless, the problem of overfitting the data remains a concern. We draw much confidence in our fit, since the results for the combination therapy directly follow from the fits of the corresponding individual treatments. The combination data were not used in the fitting.

Our model does not incorporate the effects of radiation on healthy tissues - information vital to clinically relevant determinations of optimized radiation schedules - and is fit to data from mice. Moreover, our model assumes spatial homogeneity within the tumor environment, which is almost certainly not the case. Indeed, CSCs potentially congregate within well defined CSC niches [15,34,42,48] and *survivin* expression is not uniform throughout the tumor environment [23]. The role of this spatial heterogene-

ity on the effects of radiation therapy are not well understood, and warrant further empirical and theoretical investigations.

Our results suggest that dedifferentiation may play an important role in radioresistance of CSC driven tumors, and that *survivin* may play a role in this process. Furthermore, radiation schedules optimized for use in radiation therapy alone may not be optimal when applied in combination with chemotherapeutic agents, and delaying radiation to allow tumor sensitization may prove beneficial for larger doses of radiation.

Acknowledgements: AR is grateful to an NSERC USRA scholarship. TH appreciates support through an NSERC Discovery Grant.

References

[1] R. P. Abratt, J. A. Bogart, and A. Hunter. Hypofractionated irradiation for non-small cell lung cancer. *Lung Cancer*, 36(3):225–233, 2002.

[2] L. E. Ailles and I. L. Weissman. Cancer stem cells in solid tumors. *Current Opinion in Biotechnology*, 18(5):460–466, 2007.

[3] M. Al-Hajj, M. S. Wicha, A. Benito-Hernandez, et al. Prospective identification of tumorigenic breast cancer cells. *Proceedings of the National Academy of Sciences of the United States of America*, 100(7):3983–3988, 2003.

[4] E. Alpen. *Radiation Biophysics*. Academic Press, 2nd edition, 1997.

[5] D.C. Altieri. Survivin, versatile modulation of cell division and apoptosis in cancer. *Oncogene*, 22:8581–8589, 2003.

[6] A. Amini, S. H. Lin, C. Wei, et al. Accelerated hypofractionated radiation therapy compared to conventionally fractionated radiation therapy for the treatment of inoperable non-small cell lung cancer. *Radiation Oncology*, 7(33), 2012. doi: 10.1186/1748-717X-7-33.

[7] J. W. N. Bachman and T. Hillen. Mathematical optimization of the combination of radiation and differentiation therapies for cancer. *Frontiers in Oncology*, 3(52):doi: 10.3389/fonc.2013.00052, 2013.

[8] H. Badri, K. Pitter, E. C. Holland, et al. Optimization of radiation dosing schedules for proneural glioblastoma. *Journal of Mathematical Biology*, 2015. doi: 10.1007/s00285-015-0908-x.

[9] S. Bao, Q. Wu, R.E. McLendron, et al. Glioma stem cells promote radioresistance by preferential activation of the DNA damage response. *Nature*, 444(7120):756–760, 2006.

[10] I. Borsi, A. Fasano, M. Primicerio, et al. A non-local model for cancer stem cells and the tumor growth paradox. *To appear in Mathematical Medicine and Biology*, 2015.

[11] K. P. Burnham, D. R. Anderson, and K. P. Huyvaert. AIC model selection and multimodel inference in behavioral ecology: some background, observations, and comparisons. *Behavioral Ecology and Sociobiology*, 65(1):23–35, 2011.

[12] C.L. Chaffer, I. Brueckmann, C. Scheel, et al. Normal and neoplastic nonstem cells can spontaneously convert to a stem-like state. *Proceedings of The National Academy of Sciences*, 108(19):7950–7955, 2011.

[13] P. Dahan, J. Martinez Gala, C. Delmas, et al. Ionizing radiations sustain glioblastoma cell dedifferentiation to a stem-like phenotype through survivin: Possible involvment in radioresistance. *Cell Death and Disease*, 5(11), 2014. doi: 10.1038/cddis.2014.509.

[14] A. Dawson and T. Hillen. Derivation of the tumour control probability (TCP) for a cell cycle model. *Comput. and Math. Meth. in Medicine*, 7:121–142, 2006.

[15] F. de Almeida Sassi, A.L. Brunetto, G. Schwartsmann, et al. Glioma revisited: From neurogenesis and cancer stem cells to the epigenetic regulation of the niche. *Journal of Oncology*, 2012:537861, 2012.

[16] T. Dohi, E. Beltrami, N.R. Wall, et al. Mitochondrial survivin inhibits apoptosis and promotes tumorigenesis. *Journal of Clinical Investigation*, 114(8):1117–1127, 2004.

[17] H. Enderling. Cancer stem cells: small subpopulation or evolving fraction. *Integrative Biology*, 7(1):14–23, 2015.

[18] A. Eramo, T. L. Haas, and R. De Maria. Lung cancer stem cells: tools and targets to fight lung cancer. *Oncogene*, 29(33):4625–4635, 2010.

[19] J. F. Fowler. 21 years of Biologically Effective Dose. *The British Journal of Radiology*, 83(991):554–568, 2010.

[20] R. Gomez-Casal, C. Bhattacharya, N. Ganesh, et al. Non-small cell lung cancer cells survived ionizing radiation treatment display cancer stem cell and epithelial-mesenchymal transition phenotypes. *Molecular Cancer*, 12(94), 2013. doi: 10.1186/1476-4598-12-94.

[21] J. Gong, M. M. dos Santos, C. Finlay, and T. Hillen. Are more complicated tumor control probability models better? *Math. Med. Biol.*, 30(1):1–19, 2011.

[22] P.B. Gupta, C.M. Fillmore, G. Jiang, et al. Stochastic state transitions give rise to phenotypic equilibrium in populations of cancer cells. *Cells*, 146(4):633–644, 2011.

[23] H. Guvenc, M.S. Pavlyukov, K. Joshi, et al. Impairment of glioma stem cell survival and growth by a novel inhibitor for survivin-ran protein complex. *Clinical Cancer Research*, 19(3):631–642, 2013.

[24] D. Hanahan and R. A. Weinberg. Hallmarks of cancer: The next generation. *Cell*, 144(5):646–674, 2011.

[25] L. G. Hanin. A stochastic model of tumor response to fractionated radiation: limit theorems and rate of convergence. *Math Biosci*, 91(1):1–17, 2004.

[26] T. Hillen, H. Enderling, and P. Hahnfeld. The tumor growth paradox and immune system-mediated selection for cancer stem cells. *Bulletin for Math Biology*, 75(1):161–184, 2013.

[27] T. Iwasa, I. Okamoto, M. Suzuki, et al. Radiosensitizing effect of YM155, a novel small-molecule survivin suppressant, in non-small cell lung cancer cell lines. *Clinical Cancer Research*, 14(20):6496–6504, 2008.

[28] L. Jones, P. Hoban, and P. Metcalfe. The use of the linear quadratic model in radiotherapy: a review. *Australasian Physics and Engineering Sciences in Medicine*, 24(3):132–146, 2001.

[29] J. Kang, Y. Zhang, D. A. Clump, et al. A free multi-model program for comparing linear-quadratic and non-linear quadratic models in TCP prediction of SABR-treated NSCLC. *International Journal of Radiation Oncology*Biology*Physics*, 90(1):S854–S855, 2014. Supplement.

[30] D. Klevebring, G. Rosin, R. Ma, et al. Sequencing of breast cancer stem cell populations indicates a dynamic conversion between differentiation states in-vivo. *Breast Cancer Research*, 16(4), 2014. doi: 10.1186/bcr3687.

[31] A. Konstorum, T. Hillen, and J. Lowengrub. Feedback regulation in a cancer stem cell model can cause an Allee effect. Bull. Math. Biology, 2016, to appear.

[32] C. Lagadec, E. Vlashi, L. D. Donna, et al. Radiation-induced reprogramming of breast cancer cells. *Stem Cells*, 30(5):833–844, 2012.

[33] T. Lapidot, C. Sirard, J. Vormoor, et al. A cell initiating human acute myeloid leukaemia after transplantation into scid mice. *Nature*, 367(6464):645–648, 1994.

[34] J.D. Lathia, J.M. Heddleston, M. Venere, et al. Deadly teamwork: Neural cancer stem cells and the microenvironment. *Cell Stem Cell*, 8(5):482–485, 2011.

[35] K. Leder, K. Pitter, Q. LaPlant, et al. Mathematical modeling of PDGF-driven glioblastoma reveals optimized radiation dosing schedules. *Cell*, 156(3):603–616, 2014.

[36] C. Li, D. G. Heidt, P. Dalerba, et al. Identification of pancreatic cancer stem cells. *Cancer Research*, 67(3):1030–1037, 2007.

[37] L. Maddalena. Analysis of an integro-differential system modeling tumor growth. *Applied Mathematics and Computation*, 245:152–157, 2014.

[38] N.D. Marjanovic, R.A. Weinberg, and C.L. Chaffer. Cell plasticity and heterogeneity in cancer. *Clinical Chemistry*, 59(1):168–179, 2013.

[39] T. Nakahara, A. Kita, K. Yamanaka, et al. YM155, a novel small-molecule survivin suppressant, induces regression of established human hormone-refractory prostate tumor xenografts. *Cancer Research*, 67(17):8014–8021, 2007.

[40] M. Pennati, M. Folini, and N. Zaffaroni. Targeting survivin in cancer therapy. *Expert Opinion on Therapeutic Targets*, 12(4):436–476, 2008.

[41] T. M. Phillips, W. H. McBride, and F. Pajonk. The response of $CD24^{-/low}$/CD44+ breast cancer-initiating cells to radiation. *Journal of the National Cancer Institute*, 98(24):1777–1785, 2006.

[42] J. Poleszczuk and H. Enderling. Cancer stem cell plasticity as tumor growth promoter and catalyst of population collapse. *Stem Cells International*, 2015. Article ID: 713565.

[43] A. Rauch, D. Hennig, C. Schafer, et al. Survivin and YM155: How faithful is the liaison? *Biochimica et Biophysica Acta - Reviews on Cancer*, 1845(2):202–220, 2014.

[44] U. Ricardi, S. Badellino, and A. R. Filippi. Stereotactic radiotherapy for early stage non small cell lung cancer. *Radiation Oncology Journal*, 33(2):57–65, 2015.

[45] S. Sarvi, A. C. Mackinnon, N Avlonitis, et al. CD133+ cancer stem-like cells in small cell lung cancer are highly tumorigenic and chemoresistant but sensitive to a novel neuropeptide antagonist. *Cancer Research*, 74(5):1554–1565, 2014.

[46] I. Shuryak, D. J. Carlson, M. Brown, et al. High-dose and fractionation effects in stereotactic radiation therapy: Analysis of tumor control data from 2965 patients. *Radiotherapy and Oncology*, 115(3):327–334, 2015.

[47] S. K. Singh, I. D. Clarke, M. Terasaki, et al. Identification of a cancer stem cell in human brain tumors. *Cancer Research*, 63(18):5821–5828, 2003.

[48] A. Sottoriva, P.M.A. Sloot, J.P. Medema, et al. Exploring cancer stem cell niche directed tumor growth. *Cell Cycle*, 9(8):1472–1479, 2010.

[49] K. Takahashi and S. Yamanaka. Induction of pluripotent stem cells from mouse embryonic and adult fibroblast cultures by defined factors. *Cell*, 126(4):663–676, 2006.

[50] V. Tirino, R. Camerlingo, R. Franco, et al. The role of CD133 in the identification and characterisation of tumour-initiating cells in non-small-cell lung cancer. *European Journal of Cardio-Thoracic Surgery*, 36(3):446–453, 2009.

[51] Z.A. Wang, T. Hillen. Pattern Formation for a Chemotaxis Model with Volume Filling Effects. *Chaos*, 17(3), 037108 (13 pages), 2007

[52] S. Yamanaka. Elite and stochastic models for induced pluripotent stem cell generation. *Nature*, 460(7251):49–52, 2009.

[53] H. Youssefpour, X. Li, A. Lander, et al. Multispecies model of cell lineages and feedback control in solid tumors. *Journal of Theoretical Biology*, 304:39–59, 2012.

[54] V. Y. Yu, D. Nguyen, F. Pajonk, et al. Incorporating cancer stem cells in radiation therapy treatment response modeling and the implication in glioblastoma multiforme treatment resistance. *International Journal of Radiation Oncology*Biology*Physics*, 91(4):866–875, 2015.